

Article

Attaining Ultra-Smooth 18CrNiMo7-6 Case Hardening Steel Surfaces with Chemical Mechanical Polishing

Wumao Peng¹, Yang Gao², Liang Jiang^{1,*}, Jinwei Liu¹ and Linmao Qian¹

¹ Tribology Research Institute, State Key Laboratory of Traction Power, Southwest Jiaotong University, Chengdu 610031, China

² CRRRC Qishuyan Institute Co., Ltd., Changzhou 213011, China

* Correspondence: jiangliang@swjtu.edu.cn

Abstract: Smooth surfaces are conducive to improving the lubrication of gears in mechanical systems. In this study, chemical mechanical polishing (CMP) was used to process 18CrNiMo7-6 case hardening steel, a typical material for gears. The results reveal that compared with formic acid and oxalic acid, citric acid can be used as a suitable complexing agent without causing apparent corrosion, probably due to the fact of its relatively stable adsorption. A synergistic effect exists between citric acid and H₂O₂. At pH 3, with 0.067 M citric acid and 1 wt% H₂O₂, a satisfactory CMP performance (i.e., a 514 nm/min material removal rate (MRR) and a 0.85 nm surface roughness S_a) was achieved. After polishing, no observable defects were found on the surface, and no discernible processing damage occurred to the substrate. In terms of the CMP's mechanism, iron is first oxidized to Fe²⁺ and Fe³⁺, which then react with citric acid to form complexes. On the one hand, most of the complexes may stay on the surface to prevent further corrosion and, thus, the surface quality is excellent. On the other hand, the complexes may reduce the surface integrity and, thus, the MRR is high. The findings open new avenues for attaining ultra-smooth steel surfaces with CMP through controlling corrosive wear.

Keywords: chemical mechanical polishing; gear; ultra-smooth; carboxylic acid; citric acid



Citation: Peng, W.; Gao, Y.; Jiang, L.; Liu, J.; Qian, L. Attaining Ultra-Smooth 18CrNiMo7-6 Case Hardening Steel Surfaces with Chemical Mechanical Polishing. *Lubricants* **2022**, *10*, 199. <https://doi.org/10.3390/lubricants10090199>

Received: 1 July 2022

Accepted: 10 August 2022

Published: 24 August 2022

Publisher's Note: MDPI stays neutral with regard to jurisdictional claims in published maps and institutional affiliations.



Copyright: © 2022 by the authors. Licensee MDPI, Basel, Switzerland. This article is an open access article distributed under the terms and conditions of the Creative Commons Attribution (CC BY) license (<https://creativecommons.org/licenses/by/4.0/>).

1. Introduction

18CrNiMo7-6 steel is a typical case hardening steel, which has been widely used as a raw material for key parts of large mechanical systems such as transmission gears in bogies of high-speed electric multiple units (EMUs) [1]. With the rapid development of high-speed railways in China, the running speed of EMUs will increase to 400 km/h and higher in the near future, which will certainly bring about challenges in the lubrication. In fact, rising the running speed of EMUs will increase the gear meshing frequency, and then the heat generated by friction in gear meshing will increase as well. Consequently, the oil temperature will rise, which might result in lubrication failure and serious accidents [2,3]. It may be feasible to introduce superlubricity to address the issue [4,5]. By controlling the friction coefficient to a magnitude of 0.001 or less, the heat generated in the gear meshing can be greatly reduced, and then the lubrication can be significantly improved. Li et al. [6] reported nanoscale superlubricity with a friction coefficient of 0.0003 between graphite and silica under ambient conditions, which can be attributed to the incommensurate contact between graphene layers. Zhang et al. [7] demonstrated macroscale superlubricity induced by graphene-coated surfaces under ambient conditions, and the friction coefficient could reach 0.006, greatly reducing friction and wear. However, achieving superlubricity in gear meshing can be formidable. Smooth surfaces are beneficial to the improvement of lubrication and the achievement of superlubricity ultimately by avoiding substrate asperities contact [5,8,9].

Mechanical parts, such as gears, are generally machined with cutting and grinding technologies. Researchers have devoted great effort to developing technologies that

improve machining efficiency and quality [10,11]. On this basis, it is feasible to further improve the surface quality with ultra-precision polishing. Chemical mechanical polishing (CMP) is an ultra-precision processing technology that has been intensively used in the semiconductor industry [12,13]. CMP can achieve a near-perfect smooth surface through the synergistic effect of chemical and mechanical interactions [14]. Zhang et al. [15] developed a novel environmentally friendly copper CMP slurry, consisting of colloidal silica, H_2O_2 and chitosan oligosaccharide. After CMP, an ultra-smooth surface with a surface roughness R_a of 0.444 nm was achieved. Furthermore, Zhang et al. [16] reported a novel green CMP slurry with triethanolamine as the chelating agent for sapphire. After CMP, a surface roughness R_a of 0.11 nm could be achieved. Recently, CMP has gradually been used to process steels to attain smooth surfaces in the mechanical industry [17–20]. In metal CMP slurries, complexing agents play a crucial role in enhancing material removal through complexation with metallic ions. Researchers have tried various complexing agents for mold steel and stainless steel. Zhang et al. [21] used glycine and triethanolamine as the complexing agents in acidic and alkaline slurries for S-136 plastic mold steel CMP, respectively. It was found that the slurry with SiO_2 as the abrasive and at pH 4 could achieve a satisfactory CMP performance. In addition, S-136 steel CMP was a representative oxidation–dissolution–mechanical removal process. Oxalic acid was demonstrated to be an effective complexing agent for stainless steel CMP [22–25]. Lee et al. [24] found that compared with citric acid (one hydroxyl group and three carboxyl groups) and glycine (one amino group and one carboxyl group), oxalic acid (two carboxyl groups) demonstrated better planarization quality for 304 stainless steel CMP at pH 4. With the optimized slurry, consisting of 39 wt% abrasive, 1 wt% oxalic acid, 0.03 wt% H_2O_2 and at pH 1.5, the surface roughness R_a could reach 7.8 nm. In addition, Liao et al. [26] used nicotinic acid in synergy with H_2O_2 to polish FV520B stainless steel, and a smooth surface was obtained. Our research group has deeply investigated the role of complexing agents in GCr15-bearing steel (AISI 52100) CMP. Based on the material removal rate (MRR) trend with pH, it can be concluded that the complexation efficiency of amino and carboxyl groups for iron gradually decreases as pH increases, suggesting that acidic pH is preferred for high-efficiency CMP of steels [27,28]. Although many studies pertaining to complexing agents have been reported on various types of steels, little work has been performed on 18CrNiMo7-6 steel.

In this work, 18CrNiMo7-6 steel was polished. Three typical carboxylic acids (i.e., formic acid, oxalic acid and citric acid) with different numbers of carboxyl groups were assessed as the complexing agents. Citric acid performing the weakest corrosion effect was selected. Then, the synergistic effect between citric acid and H_2O_2 was investigated in depth. The corresponding CMP mechanism was put forward. The related experimental results and discussion may suggest that the CMP performance of steels can be tuned by controlling the corrosive wear through varying the carbon chain length of carboxylic acids. Moreover, citric acid with three additional carbon atoms in addition to carboxylic groups in synergy with H_2O_2 can efficiently achieve an excellent surface quality for 18CrNiMo7-6 steel.

2. Experimental Methods

The 18CrNiMo7-6 steel used in this study was provided by China Railway Rolling Stock Corporation (CRRC) Qishuyan Institute Co., Ltd. As reported, the yield strength was approximately 855 MPa [29]. The energy-dispersive X-ray spectroscopy (EDS), scanning electron microscopy (SEM, measured with Apreo S, Thermo Fisher Scientific) and metallographic microscopy (measured with Axio Lab.A1, Carl Zeiss) characterization results of 18CrNiMo7-6 steel are displayed in Figure 1. As shown in the EDS result in Figure 1a, iron accounts for approximately 95.6 wt% and, therefore, iron will mainly be discussed in the following investigation. Moreover, the chemical composition measured with EDS over the surface area shown in Figure 1b meets the standard of BS EN 10084:2008. As shown in Figure 1c, the major metallographic structure was lath martensite [30,31].

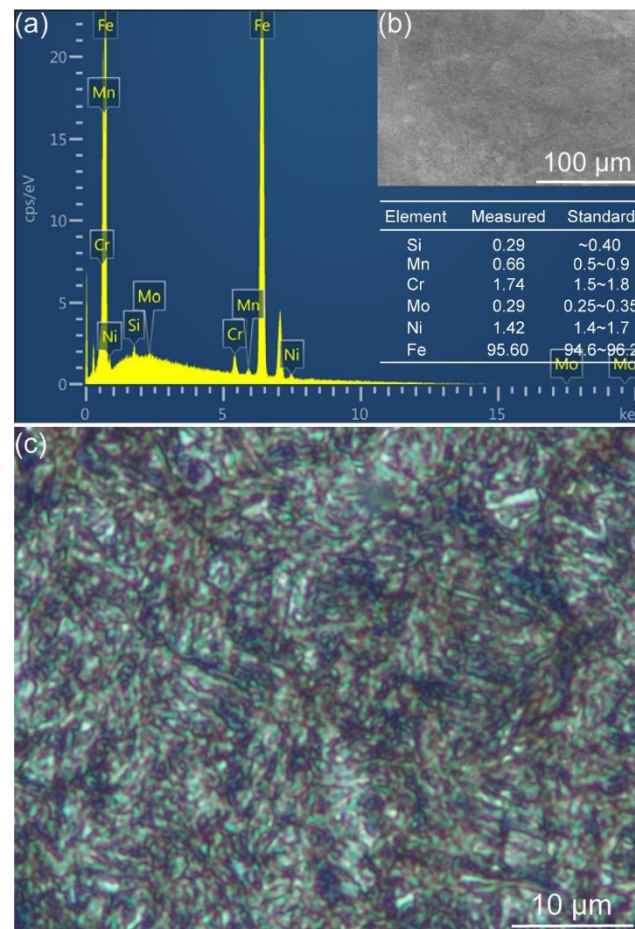


Figure 1. Characterization results of 18CrNiMo7-6 steel: (a) the EDS result of the surface area shown in (b); (b) the SEM image; (c) the metallographic structure.

In the CMP experiments, a 18CrNiMo7-6 steel disc, 50.8 mm in diameter, was polished with an automatic pressure lapping/polishing machine (UNIPOL-1200S, Shenyang Kejing Automatic Equipment Co., Ltd., Shenyang, Liaoning, China). The CMP slurries' composition is listed in Table 1. The chemical reagents were purchased from Sinopharm Chemical Reagent Co., Ltd. (Shanghai, China).

Table 1. CMP slurries' composition.

Component	Chemical
Abrasive	Colloidal silica (YZ8040, Shanghai YZ-Lapping Material Co., Ltd., Shanghai, China)
Complexing agent	Formic acid, oxalic acid or citric acid
Oxidant	H ₂ O ₂
pH buffer	HNO ₃ and KOH
Others	Ultrapure water

The CMP conditions are given in Table 2. After CMP, the disc was quickly cleaned with water and dried. The weight loss was measured with a microbalance (1 μg readability, ME36S, Sartorius), and the MRR was calculated as follows: $MRR = \Delta m / (\rho \times A \times t)$, where Δm is the weight loss after CMP; ρ is the density of the 18CrNiMo7-6 steel, which was 7.8 g/cm³; A is the polishing area, which was 2027 mm²; t is the time of each polishing, which was 1 min. The surface morphology and surface roughness S_a over 97.9 × 97.9 μm scan area were measured with an optical 3D surface profiler (SuperView W1, Chotest Technology Inc., Shenzhen, China). Each slurry was repeated four times.

Table 2. CMP conditions.

Parameter	Value
Set pressure displayed on the panel	5 kg
Carrier speed	60 rpm
Platen speed	60 rpm
Slurry flow rate	100 mL/min
Time of each polishing	1 min
Polishing pad	IC1010/Suba-IV polyurethane pad

In addition, static etching experiments were carried out to compare the chemical aggressiveness of different carboxylic acids and to explain the corrosive wear mechanism in CMP. Like the MRR, the static etching rate (SER) was calculated according to the above weight loss method. Specifically, the sample size was $29.8 \times 29.8 \times 4.7$ mm. The etching time was 3 min.

To observe the surface and subsurface more intuitively, the polished 18CrNiMo7-6 steel sample was first cut with a focused ion beam. Then, the cross-section was characterized in detail with high-resolution transmission electron microscopy (HRTEM, JEM-2800F, JEOL), selected area electron diffraction (SAED), and EDS. Furthermore, X-ray photoelectron spectroscopy (XPS, Axis Ultra DLD, Kratos) was used to analyze the chemical elements and valence states of the polished 18CrNiMo7-6 steel surface.

3. Results and Discussion

3.1. The Performance of Three Typical Carboxylic Acids in 18CrNiMo7-6 Steel CMP

Carboxylic acids can be used as effective complexing agents for steel CMP to boost the MRR. However, for certain steels, such as 18CrNiMo7-6, it is necessary to find a suitable carboxylic acid. On the one hand, the MRR can be greatly enhanced. On the other hand, the surface quality can be maintained without causing severe corrosion. In this section, three typical carboxylic acids with different numbers of carboxylic groups, including formic acid, oxalic acid and citric acid, were added to the baseline slurry separately, and the performance of the CMP was examined. Here, the baseline slurry consisted of 2 wt% colloidal silica and 0.1 wt% H_2O_2 at pH 3. In particular, for comparison, the carboxylic group's concentration was strictly controlled at 0.2 M for all cases. The CMP results are shown in Figure 2. As shown in Figure 2a, formic acid, oxalic acid and citric acid are representative of monocarboxylic acid, dicarboxylic acid and tricarboxylic acid, respectively. As shown in Figure 2b, after adding the carboxylic acids, the MRR of the 18CrNiMo7-6 steel was greatly enhanced. However, for formic acid and oxalic acid, although the MRR was quite high, the surface, especially the disc's edge area, became relatively rough, as shown in Figure 2c, and the surface roughness S_a at the disc's edge became larger than 100 nm as shown in Figure 2b. Surprisingly, for citric acid, the surface was smooth and uniform across the whole disc.

Furthermore, static etching experiments were carried out to preliminarily explore the reason for the distinct CMP performances among formic acid, oxalic acid and citric acid. The results are shown in Figure 3. As can be seen, the SER of 18CrNiMo7-6 steel displayed a similar changing trend as the above MRR. After immersion in a slurry containing formic acid or oxalic acid, the SER was high, but the surface became black and rough, which was probably caused by the synergistic effect of oxidation from a low content of H_2O_2 (0.1 wt%) and complexation from formic acid or oxalic acid. By contrast, after immersion in the slurry containing citric acid, the SER slightly increased compared to the baseline slurry, and the surface remained almost unchanged. Moschona et al. [32] reported that phosphonate with a longer carbon chain could result in more stable adsorption on the carbon steel surface due to the more negative standard free energy of adsorption and denser surface film. In our case, compared with formic acid and oxalic acid, citric acid possessed three extra carbon atoms in addition to its carboxylic groups. Therefore, referring to the conclusion of Moschona et al., it can be inferred that the low SER of citric acid is likely from

its relatively stable adsorption on the 18CrNiMo7-6 steel surface. In addition, static etching experiments were further conducted with acetic acid that contained one additional carbon atom than the formic acid. The SER was low, and the surface showed no signs of apparent corrosion, verifying the influence of the carbon chain's length to some extent. Considering that steel CMP is a typical corrosive wear process [21], the surface quality of 18CrNiMo7-6 steel after polishing with citric acid remained almost unchanged accordingly due to the slight corrosion.

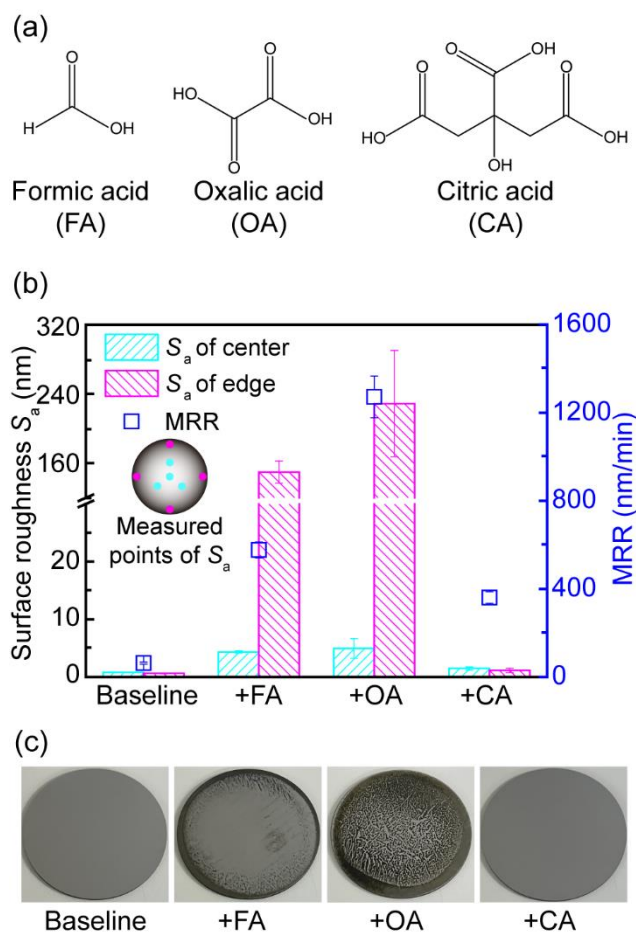


Figure 2. Performance of three typical carboxylic acids in the CMP of 18CrNiMo7-6 steel: (a) the molecular structures of the three carboxylic acids; (b) the MRR and surface roughness S_a results; (c) photographs of the discs after polishing.

For application in gear CMP, slurries may sputter to other areas of the gear curve surface. The balance between oxidation and complexation may vary from the polishing area, and corrosion may occur if the complexing agent is not appropriate. Based on the CMP and static etching results, citric acid, one of the most common carboxylic acids in our daily life, can be used as a suitable and green complexing agent for CMP of 18CrNiMo7-6 steel. In synergy with H_2O_2 , citric acid can greatly enhance the MRR of 18CrNiMo7-6 steel without sacrificing the surface quality. In the following sections, the synergistic effect was deeply investigated.

3.2. Synergistic Effect of Citric Acid and H_2O_2 on the CMP of 18CrNiMo7-6 Steel

Normally, in metal CMP, a synergistic effect exists between the complexing agent and oxidant, through which the CMP's performance can be significantly improved, especially the MRR. Therefore, in this section, the synergistic effect of citric acid and H_2O_2 on the CMP of 18CrNiMo7-6 steel was first examined. Specifically, here, the baseline slurry (denoted as slurry 1) was composed of 2 wt% colloidal silica at pH 3; Slurry 2 contained an additional

0.067 M citric acid; Slurry 3 contained an additional 1 wt% H_2O_2 ; Slurry 4 contained an additional 0.067 M citric acid and 1 wt% H_2O_2 . The MRR results are shown in Figure 4. Compared with the MRR of the baseline slurry, after adding citric acid in Slurry 2 or H_2O_2 in Slurry 3, the MRR slightly decreased. In sharp contrast, after adding both citric acid and H_2O_2 in Slurry 4, the MRR increased from 59 to 514 nm/min, and the increment was approximately that of eight times, confirming that a strong synergistic effect exists between citric acid and H_2O_2 .

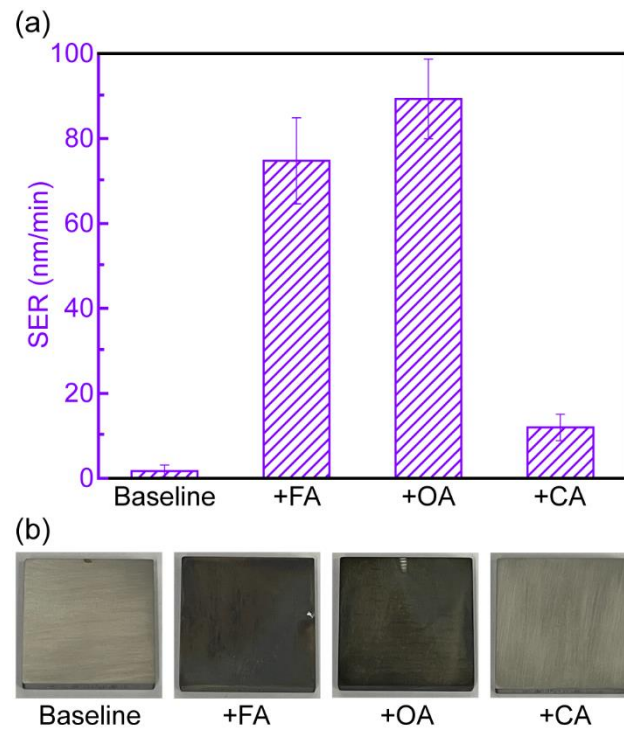


Figure 3. Performances of three typical carboxylic acids in static etching experiments on 18CrNiMo7-6 steel: (a) SER results; (b) photographs of the samples after the static etching experiments.

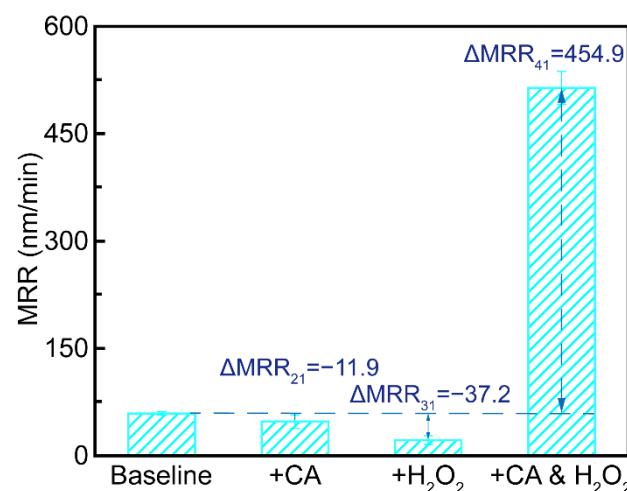


Figure 4. Preliminary investigations on the synergistic effect of citric acid and H_2O_2 on the CMP of 18CrNiMo7-6 steel; ΔMRR_{i1} represents the MRR's difference between Slurry i and Slurry 1 ($i = 2, 3$ and 4).

Furthermore, to determine an appropriate synergistic effect between citric acid and H_2O_2 for the CMP of 18CrNiMo7-6 steel, in the presence of citric acid, the effect of the H_2O_2 concentration on the CMP's performance on 18CrNiMo7-6 steel at different pHs

was investigated. The slurries were composed of 2 wt% colloidal silica, 0.067 M citric acid and different concentrations of H_2O_2 at different pHs. The MRR results are shown in Figure 5. As can be seen, the MRR decreased as the pH increased overall. According to the pH-potential diagram of the iron–water system [33–35], pH can influence the surface status. With an increasing pH, iron is more inclined to form passive oxides. The surface film becomes more difficult to remove. Therefore, the MRR decreases. Similar phenomena were reported in our previously published articles [17,18,27,28]. Moreover, the MRR first increased and then decreased as the H_2O_2 concentration increased for all testes pHs. Specifically, at pH 3, with increasing H_2O_2 , the MRR first rose from 47 nm/min to a maximum of 734 nm/min when the H_2O_2 concentration increased from 0 to 0.5 wt%, and then gradually decreased to 78 nm/min when the H_2O_2 concentration further increased to 2 wt%. Noticeably, after adding only 0.5 wt% H_2O_2 , the MRR increased by 15 times.

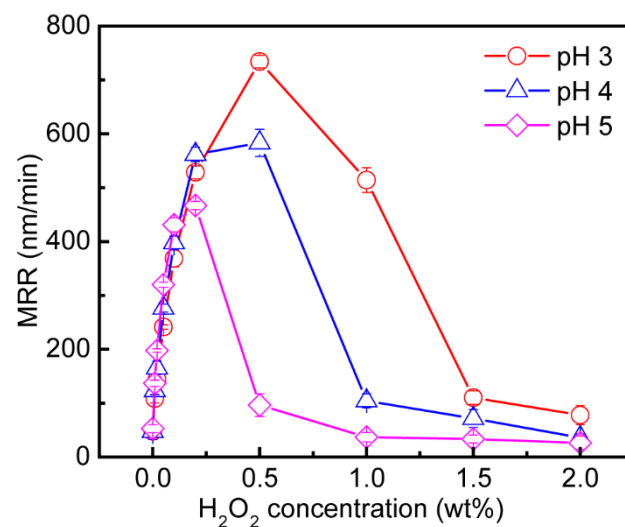


Figure 5. Synergistic effect of citric acid and H_2O_2 on the CMP of 18CrNiMo7-6 steel at different pHs.

The corresponding photographs and optical images of the 18CrNiMo7-6 steel discs after polishing at pH 3 are shown in Figure 6. Combined with Figure 2c, no observable corrosion or scratches can be observed on the entire 18CrNiMo7-6 steel disc's surface for all H_2O_2 concentrations.

The corresponding surface roughness S_a and three-dimensional surface morphology results of 18CrNiMo7-6 steel after polishing at pH 3 are shown in Figure 7. As shown in Figure 7a, overall, the surface roughness S_a decreased from 2.35 to 0.42 nm as the H_2O_2 concentration increased from 0 to 2 wt%. However, as shown in the inset of Figure 7a, after adding a very low concentration of H_2O_2 , such as 0.01 wt%, the surface roughness S_a slightly increased, which might be attributed to the fact that such a low content of H_2O_2 cannot oxidize the whole disc's surface adequately, and the surface film can be nonuniform, resulting in uneven removal [36]. As shown in Figure 7b, with the increased H_2O_2 concentration, the peak-to-valley height of the surface morphology followed the same trend as the surface roughness S_a . In particular, at 1 wt% H_2O_2 , the peak-to-valley height reached less than 10 nm, and no micron-scale defects could be observed on the surface.

To conclude, citric acid can be used as a suitable complexing agent for the CMP of 18CrNiMo7-6 steel. By tuning the synergistic effect between citric acid and H_2O_2 via adjusting the H_2O_2 concentration, the CMP's performance can be regulated. Comprehensively considering CMP efficiency and surface quality, the slurry containing 0.067 M citric acid and 1 wt% H_2O_2 exhibited a satisfactory CMP performance, i.e., a 514 nm/min MRR and a 0.85 nm surface roughness S_a .

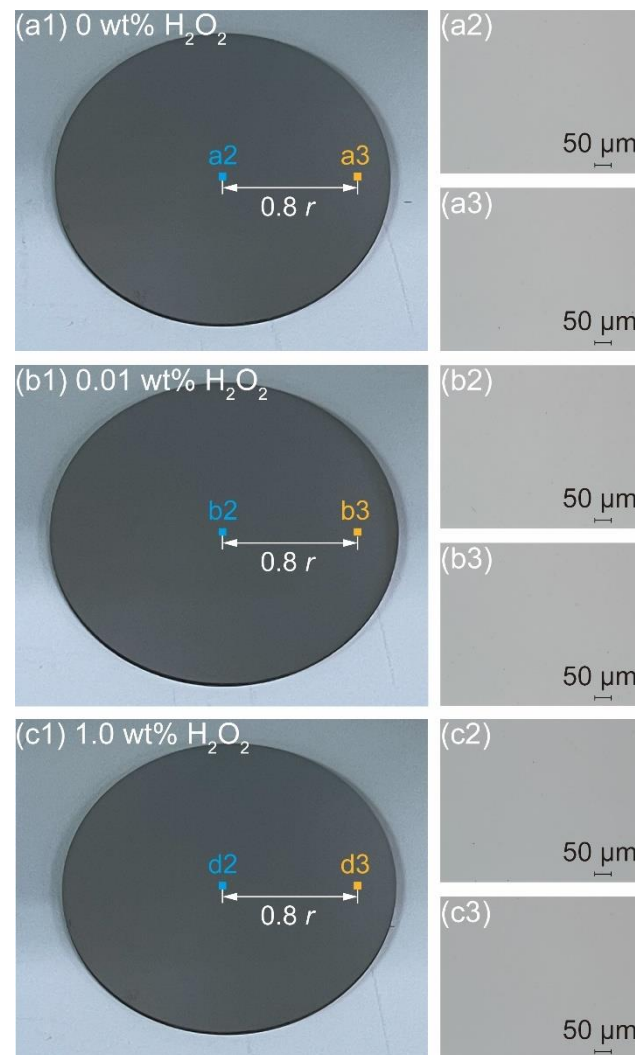


Figure 6. Photographs and optical images of the 18CrNiMo7-6 steel discs after polishing with the slurries containing different concentrations of H_2O_2 at pH 3: (a1–a3) 0 wt% H_2O_2 ; (b1–b3) 0.01 wt% H_2O_2 ; (c1–c3) 1 wt% H_2O_2 .

3.3. Characterization of the Surface Film of 18CrNiMo7-6 Steel

In this section, to reveal CMP's mechanism, the surface and subsurface of 18CrNiMo7-6 steel after polishing were characterized by HRTEM, SAED, EDS and XPS. For preparation, the sample was first polished with the slurry containing 2 wt% colloidal silica, 0.067 M citric acid, and 1 wt% H_2O_2 at pH 3, and then it was cleaned with water and dried. The HRTEM results are shown in Figure 8. Through the HRTEM observation, there was a thin surface film that formed on the top of the substrate. The thicknesses of the surface film were approximately 3 nm at different positions, further confirming that the surface morphology was uniform and smooth. In addition, the surface film was amorphous, while the substrate had an intact crystal structure, showing that the CMP did not cause processing damage to the 18CrNiMo7-6 steel's substrate.

The SAED results of the surface film and substrate are shown in Figure 9. The different diffraction patterns further confirm that the surface film was amorphous, while the substrate was crystalline. Moreover, the 18CrNiMo7-6 steel substrate had a body-centered cubic crystal structure [37]. The crystal lattice constant was calculated as follows [38]: $a = d_{hkl} \times (h^2 + k^2 + l^2)^{1/2}$, where a is the crystal lattice constant; d_{hkl} is the crystal plane spacing, as shown in Figure 9(c1); (h , k and l) is the crystal plane index as shown in Figure 9(c2). After

calculation, the crystal lattice constants of the 18CrNiMo7-6 steel substrate were 0.27 nm, 0.27, and 0.28 nm, respectively, which are close to the predicted results by Liu et al. [39].

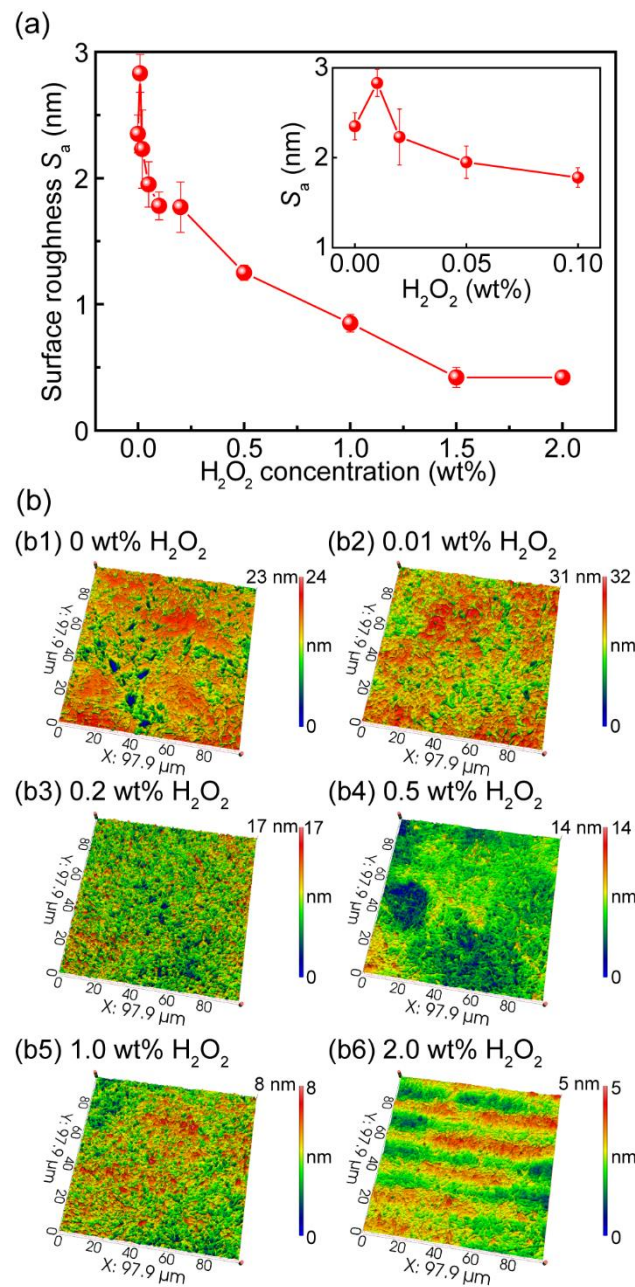


Figure 7. Surface roughness S_a and three-dimensional surface morphology results of 18CrNiMo7-6 steel after polishing with the slurries containing different concentrations of H_2O_2 at pH 3: (a) The surface roughness S_a results; (b1–b6) The three-dimensional surface morphology results.

The EDS results are shown in Figure 10. As shown in Figure 10c,d, the sample was covered with a protective glue layer that contained C and O. As shown in Figure 10a,b,d,e, as the detection depth increased from 7.97 to 12.6 nm, the concentration of O increased from 13.1 wt% to 32.1 wt%, and the concentration of Fe increased from 3.57 wt% to 42.59 wt%, revealing that the surface film can be primarily composed of iron oxides. However, it is difficult to identify whether the low content of C in the surface film was from the glue layer or complex compounds of iron and citric acid, which can be resolved by the following XPS instead. As shown in Figure 10e–j, the 18CrNiMo7-6 steel substrate mainly contained

evenly distributed Fe, Cr, Ni, Mo, Mn and Si, which is in accord with the standard of BS EN 10084:2008.

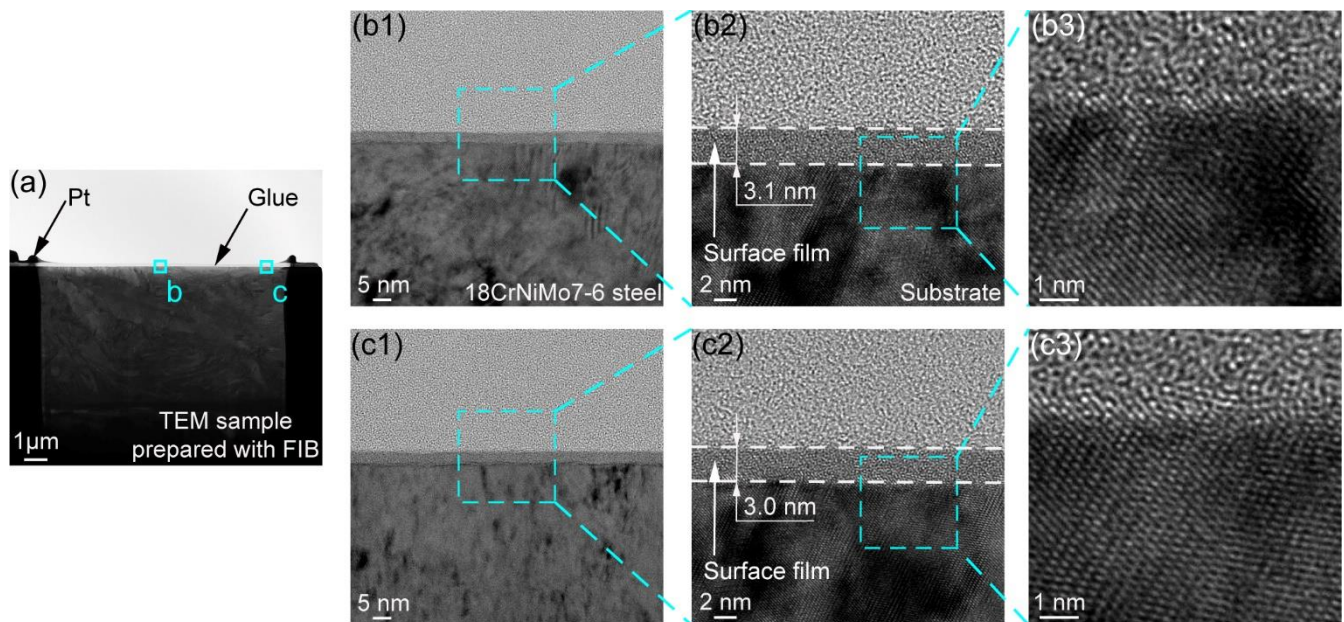


Figure 8. HRTEM results of the polished 18CrNiMo7-6 steel sample: (a) The cross-section of the TEM sample; (b1–b3) The HRTEM images at the position “b” shown in (a); (c1–c3) The HRTEM images at the position “c” shown in (a).

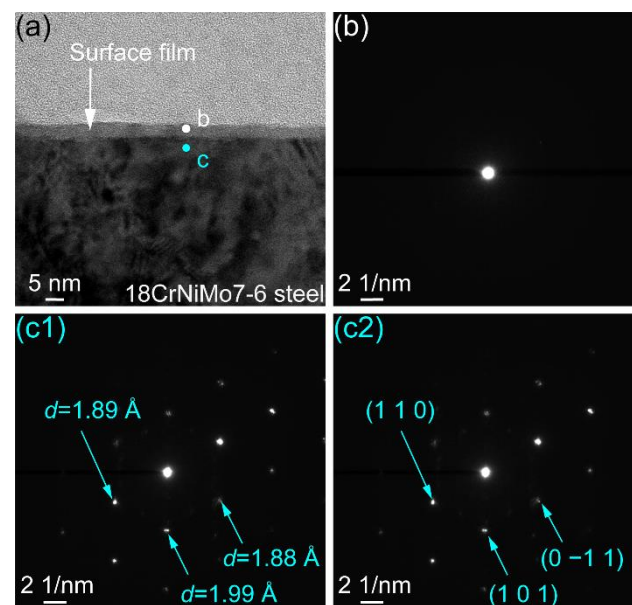


Figure 9. SAED results of the polished 18CrNiMo7-6 steel sample: (a) HRTEM image; (b) diffraction pattern on the surface film at position b; (c1) and (c2) the diffraction pattern of the substrate at position c.

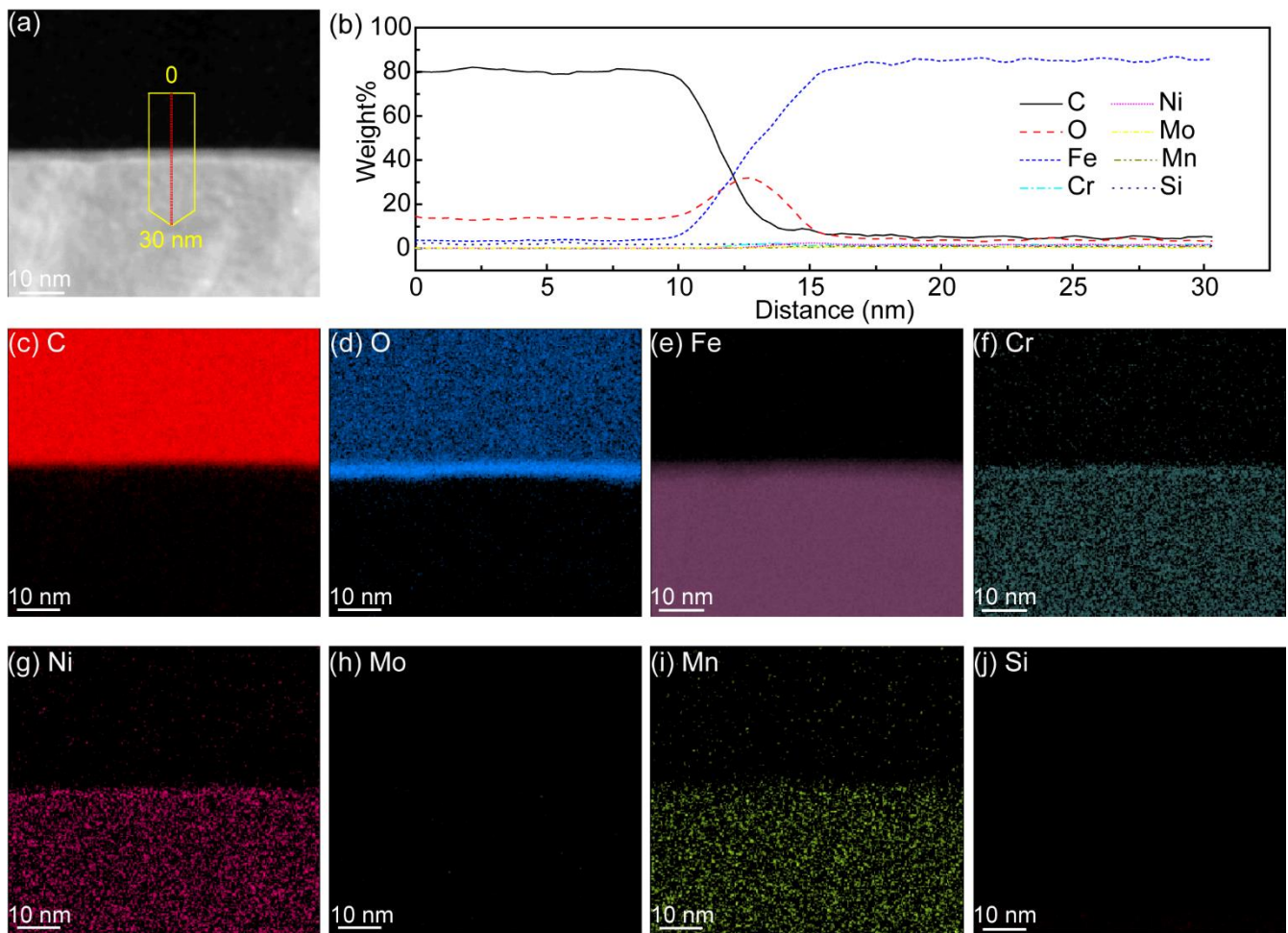


Figure 10. EDS results of the polished 18CrNiMo7-6 steel sample: (a) scanning TEM dark-field image; (b) weight distributions of C, O, Fe, Cr, Ni, Mo, Mn and Si in the marked areas shown in (a); (c–j) EDX maps of C, O, Fe, Cr, Ni, Mo, Mn and Si, respectively.

XPS was used to further analyze the chemical composition of the 18CrNiMo7-6 steel surface after polishing. The XPS results are shown in Figure 11. As shown in Figure 11a, the Fe($2p_{3/2}$) spectrum showed three peaks with binding energies of 711.5, 709.3 and 706.4 eV, which can be from Fe³⁺ (17.11%), Fe²⁺ (62.61%) and Fe⁰ (20.28%), respectively [40–42]. As shown in Figure 11b, the Cr($2p_{3/2}$) spectrum revealed one peak with a binding energy of 576.0 eV, which can correspond to chromium compounds [43]. As shown in Figure 11c, the C(1s) spectrum can be fitted to four peaks with binding energies of 288.1, 285.6, 284.6 and 282.8 eV, which can correspond to C=O, C-O, C-C and iron carbides [44]. As shown in Figure 11d, the O(1s) spectrum showed four peaks with binding energies of 532.7, 531.5, 531.1 and 529.5 eV, which can be from C=O, C-O, OH⁻ and O²⁻, respectively [44,45]. Combined with the above EDS results, it can be concluded that the polished 18CrNiMo7-6 steel surface was mainly composed of iron oxides and a small number of complex compounds of iron and citric acid.

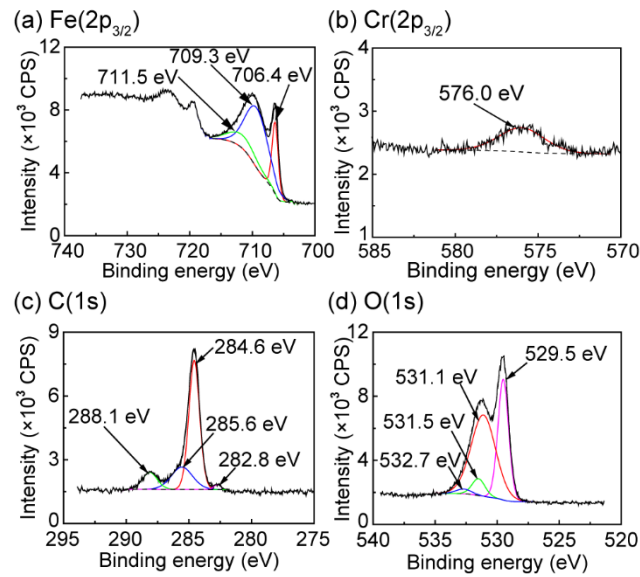


Figure 11. XPS results of the polished 18CrNiMo7-6 steel surface: (a) Fe(2p_{3/2}); (b) Cr(2p_{3/2}); (c) C(1s); (d) O(1s).

3.4. Action Mechanism of Citric Acid and H₂O₂ in the CMP of 18CrNiMo7-6 Steel

Based on the experimental results obtained so far and the relevant literature, a preliminary CMP mechanism via the synergistic effect of citric acid and H₂O₂ can be described as follows. A corresponding schematic illustration is shown in Figure 12.

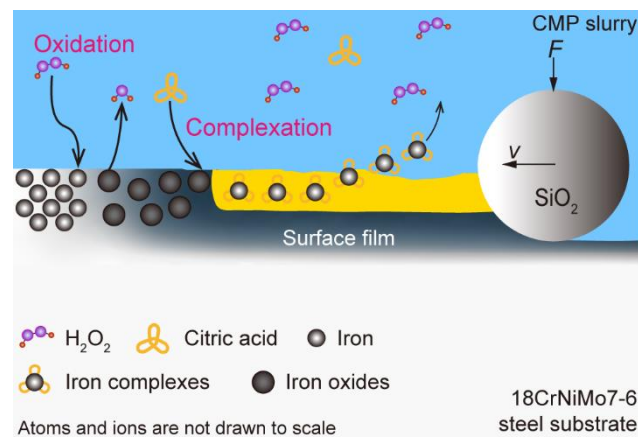
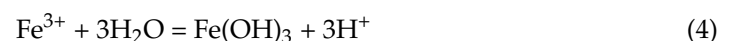
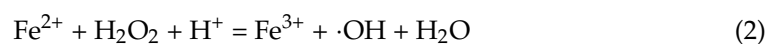
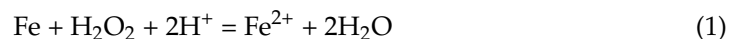


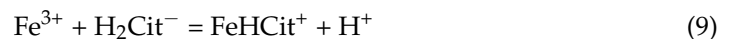
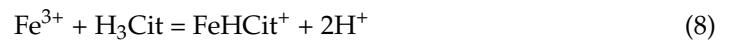
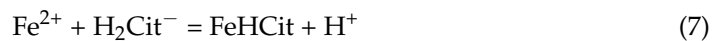
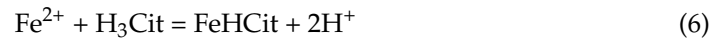
Figure 12. Action mechanism of citric acid and H₂O₂ in the CMP of 18CrNiMo7-6 steel.

As aforementioned, iron takes up approximately 95 wt% of 18CrNiMo7-6 steel and, therefore, iron is mainly discussed. During the CMP process, with a relatively high concentration of H₂O₂, such as 1 wt%, iron is first oxidized to Fe²⁺ and Fe³⁺. Then, uniform and compact iron oxides are gradually formed on the surface as revealed in the above HRTEM and XPS results. In particular, if no complexing agent was added, the surface grew compact, and the MRR decreased as shown in Figure 4. The oxidation reactions, including the Fenton reaction, can be depicted as follows [46–48]:





When adding an effective complexing agent citric acid, it can react with Fe^{2+} and Fe^{3+} on the surface, most likely at the outmost surface, to form complex compounds. At pH 3, citric acid mainly exists in the forms of H_3Cit (neutral molecule: 56.9 at%) and H_2Cit^- (42.4 at%) [49]. The complexation reactions can be depicted as follows [34,50]:



During the CMP process, the statistically average interval between consecutive asperity-steel surface contacts is approximately microseconds to milliseconds [51,52]. In such a short period, it is highly possible that complex compounds, such as FeHCit and FeCit , do not dissolve in the slurry and drain out in time, but most of them remain on the surface due to the relatively stable adsorption as explained in the above static etching results [53]. As a result, the chemical additives, H_2O_2 and citric acid, cannot further penetrate the substrate, and no obvious corrosion occurs; thus, the surface quality is excellent after polishing. Meanwhile, the formation of complex compounds can reduce the surface's integrity. The surface, especially the outmost surface, becomes fragile, and it can be removed by silica particles readily. Therefore, the MRR is high.

Combined with our previous research [27,54], the findings suggest that carboxylic acids can be used as promising complexing agents for steel's CMP. The carbon chain length of carboxylic acids had a significant influence on the CMP's performance, especially the surface quality. With a suitable carbon chain length, an excellent surface quality and a high MRR can be achieved at the same time. For 18CrNiMo7-6 steel, citric acid with an extra three carbon atoms in addition to carboxylic groups in synergy with H_2O_2 can lead to a satisfactory CMP performance without obvious corrosion. To completely avoid corrosion, corrosion inhibitors can be further added [55,56]. Hopefully, the optimized slurries working with a small bonnet tool can be used for the numerical control of sub-aperture CMP of a real gear curve surface in the near future [57].

4. Conclusions

In this study, the synergistic effect of citric acid and H_2O_2 on the CMP of 18CrNiMo7-6 case hardening steel was investigated in detail. With a proper synergistic effect, an ultra-smooth 18CrNiMo7-6 steel surface can be obtained. Based on the results and discussion above, the following conclusions can be drawn:

- (1) In the presence of 0.1 wt% H_2O_2 at pH 3, compared with formic acid and oxalic acid, citric acid with three additional carbon atoms in addition to carboxylic groups can enhance the MRR of 18CrNiMo7-6 steel without sacrificing surface quality, which may be ascribed to the relatively stable adsorption on the steel's surface. Citric acid can be used as a suitable complexing agent for the CMP of 18CrNiMo7-6 steel;
- (2) An evident synergistic effect existed between citric acid and H_2O_2 . Under acidic conditions, as the H_2O_2 concentration increased, the MRR of the 18CrNiMo7-6 steel first increased and then gradually decreased, while the surface roughness decreased on the whole. No obvious corrosion and scratches could be found on the surface. Moreover, a satisfactory CMP performance (i.e., 514 nm/min MRR and 0.85 nm surface roughness S_a), was attained with the slurry containing 2 wt% colloidal silica, 0.067 M citric acid and 1 wt% H_2O_2 at pH 3. No observable processing damage was generated in the substrate;

- (3) During CMP, iron was first oxidized to Fe^{2+} and Fe^{3+} by H_2O_2 . Then, the citric acid reacted with Fe^{2+} and Fe^{3+} on the surface to form complexes such as FeHCit and FeCit . Between the two consecutive mechanical abrasions, the complexes may not have dissolved in the slurry in time, and much may have remained on the surface preventing further corrosion, thereby leading to a surface roughness that was low. However, the surface integrity may have been weakened by the complexes and, therefore, the MRR was high.

Author Contributions: Conceptualization, L.J.; formal analysis, W.P., J.L. and L.J.; investigation, W.P.; resources, Y.G., L.J. and L.Q.; writing—original draft preparation, W.P.; writing—review and editing, L.J. and L.Q.; funding acquisition, L.J. and L.Q. All authors have read and agreed to the published version of the manuscript.

Funding: This research was supported by the National Key R&D Program of China (2020YFA0711001), National Natural Science Foundation of China (51975488 and 51991373), National Key R&D Program of China (2018YFB2000400), Fundamental Research Funds for the Central Universities (2682021CG011), and Beijing Key Laboratory of Long-Life Technology of Precise Rotation and Transmission Mechanisms (BZ0388201902).

Institutional Review Board Statement: Not applicable.

Informed Consent Statement: Not applicable.

Data Availability Statement: The data presented in this study are available on request from the corresponding author.

Acknowledgments: We would like to thank the Analytical & Testing Center of Sichuan University for the XPS work, and we are grateful to Shuguang Yan for his help with the XPS analysis.

Conflicts of Interest: The authors declare no conflict of interest.

References

1. Ding, H.; Lei, L.; Qin, M.; Wang, G. Parametric Design on Solving the Maximum Deformation of Traction Helical Gear on Locomotive. *J. Phys. Conf. Ser.* **2020**, *1650*, 022020. [[CrossRef](#)]
2. Höhn, B.R.; Michaelis, K. Influence of oil temperature on gear failures. *Tribol. Int.* **2004**, *37*, 103–109. [[CrossRef](#)]
3. Kr Singh, D.; Kurien, J.; Villayamore, A. Study and analysis of wind turbine gearbox lubrication failure and its mitigation process. *Mater. Today Proc.* **2021**, *44*, 3976–3983. [[CrossRef](#)]
4. Li, J.; Luo, J. Advancements in superlubricity. *Sci. China Technol. Sci.* **2013**, *56*, 2877–2887. [[CrossRef](#)]
5. Xu, J.; Li, J. New achievements in superlubricity from international workshop on superlubricity: Fundamental and applications. *Friction* **2015**, *3*, 344–351. [[CrossRef](#)]
6. Li, J.; Gao, T.; Luo, J. Superlubricity of Graphite Induced by Multiple Transferred Graphene Nanoflakes. *Adv. Sci.* **2018**, *5*, 1700616. [[CrossRef](#)] [[PubMed](#)]
7. Zhang, Z.; Du, Y.; Huang, S.; Meng, F.; Chen, L.; Xie, W.; Chang, K.; Zhang, C.; Lu, Y.; Lin, C.-T.; et al. Macroscale Superlubricity Enabled by Graphene-Coated Surfaces. *Adv. Sci.* **2020**, *7*, 1903239. [[CrossRef](#)]
8. Zhou, F.; Adachi, K.; Kato, K. Sliding friction and wear property of a-C and a-CN_x coatings against SiC balls in water. *Thin Solid Films* **2006**, *514*, 231–239. [[CrossRef](#)]
9. Liu, Y.; Li, J.; Ge, X.; Yi, S.; Wang, H.; Liu, Y.; Luo, J. Macroscale Superlubricity Achieved on the Hydrophobic Graphene Coating with Glycerol. *ACS Appl. Mater. Interfaces* **2020**, *12*, 18859–18869. [[CrossRef](#)]
10. Yang, M.; Li, C.; Said, Z.; Zhang, Y.; Li, R.; Debnath, S.; Ali, H.M.; Gao, T.; Long, Y. Semiempirical heat flux model of hard-brittle bone material in ductile microgrinding. *J. Manuf. Processes* **2021**, *71*, 501–514. [[CrossRef](#)]
11. Tang, L.; Zhang, Y.; Li, C.; Zhou, Z.; Nie, X.; Chen, Y.; Cao, H.; Liu, B.; Zhang, N.; Said, Z.; et al. Biological Stability of Water-Based Cutting Fluids: Progress and Application. *Chin. J. Mech. Eng.* **2022**, *35*, 3. [[CrossRef](#)]
12. Speed, D.; Westerhoff, P.; Sierra-Alvarez, R.; Draper, R.; Pantano, P.; Aravamudhan, S.; Chen, K.L.; Hristovski, K.; Herckes, P.; Bi, X.; et al. Physical, chemical, and in vitro toxicological characterization of nanoparticles in chemical mechanical planarization suspensions used in the semiconductor industry: Towards environmental health and safety assessments. *Environ. Sci. Nano* **2015**, *2*, 227–244. [[CrossRef](#)]
13. Lee, H. Environmental impact of concentration of slurry components in thick copper CMP. *Int. J. Precis. Eng. Manuf.-Green Technol.* **2017**, *4*, 13–18. [[CrossRef](#)]
14. Li, J.; Liu, Y.; Dai, Y.; Yue, D.; Lu, X.; Luo, J. Achievement of a near-perfect smooth silicon surface. *Sci. China Technol. Sci.* **2013**, *56*, 2847–2853. [[CrossRef](#)]

15. Zhang, Z.; Cui, J.; Zhang, J.; Liu, D.; Yu, Z.; Guo, D. Environment friendly chemical mechanical polishing of copper. *Appl. Surf. Sci.* **2019**, *467–468*, 5–11. [[CrossRef](#)]
16. Zhang, Z.; Liu, J.; Hu, W.; Zhang, L.; Xie, W.; Liao, L. Chemical mechanical polishing for sapphire wafers using a developed slurry. *J. Manuf. Processes* **2021**, *62*, 762–771. [[CrossRef](#)]
17. Jiang, L.; He, Y.; Luo, J. Effects of pH and oxidizer on chemical mechanical polishing of AISI 1045 steel. *Tribol. Lett.* **2014**, *56*, 327–335. [[CrossRef](#)]
18. Jiang, L.; He, Y.; Luo, J. Chemical mechanical polishing of steel substrate using colloidal silica-based slurries. *Appl. Surf. Sci.* **2015**, *330*, 487–495. [[CrossRef](#)]
19. Jiang, L.; He, Y.; Yang, Y.; Luo, J. Chemical mechanical polishing of stainless steel as solar cell substrate. *ECS J. Solid State Sci. Technol.* **2015**, *4*, P162–P170. [[CrossRef](#)]
20. Jiang, L.; Yao, W.; He, Y.; Cheng, Z.; Yuan, J.; Luo, J. An experimental investigation of double-side processing of cylindrical rollers using chemical mechanical polishing technique. *Int. J. Adv. Manuf. Technol.* **2016**, *82*, 523–534. [[CrossRef](#)]
21. Zhang, D.; Liu, J.; Chen, Y.; Wang, M.; Ge, X. Investigation on S-136 steel surface planarization by chemical mechanical polishing. *Microelectron. Eng.* **2015**, *134*, 47–53. [[CrossRef](#)]
22. Wang, Y.; Xu, R.; Wang, Y.; Wang, Z.; Su, J. Study on Dispersant of Hydrogen Peroxide-Oxalic Acid Polishing Slurry in Chemical Mechanical Polishing of 304 Stainless Steel. *J. Phys. Conf. Ser.* **2020**, *1622*, 012097. [[CrossRef](#)]
23. Yongsheng, W.; Haixu, L.; Xiaojun, C.; Zhankui, W.; Jianxiu, S. Selection of Surfactants for Hydrogen peroxide-oxalic acid Polishing Slurry in Chemical Mechanical Polishing of 304 Stainless Steel. *J. Phys. Conf. Ser.* **2020**, *1681*, 012013. [[CrossRef](#)]
24. Lee, D.; Kim, H.; Pak, B.; Kim, D.; Jeong, H.; Lee, H. Electrochemical Analysis of the Slurry Composition for Chemical Mechanical Polishing of Flexible Stainless-Steel Substrates. *J. Frict. Wear* **2017**, *38*, 482–489. [[CrossRef](#)]
25. Kim, T.; Lee, H. Preliminary Study on Fluidized Bed Chemical Mechanical Polishing (FB-CMP) Process for Stainless Steel 304 (SS304). *Micromachines* **2020**, *11*, 705. [[CrossRef](#)]
26. Liao, L.; Zhang, Z.; Liu, J.; Li, Y.; Cui, X.; Liu, L. A novel process of chemical mechanical polishing for FV520B steel. *J. Manuf. Processes* **2020**, *59*, 51–57. [[CrossRef](#)]
27. Liu, J.; Jiang, L.; Wu, H.; Zhong, X.; Qian, L. Performance of Carboxyl Groups in Chemical Mechanical Polishing of GCr15 Bearing Steel: Effects of Carbon Chain Length and pH. *Tribol. Lett.* **2021**, *69*, 161. [[CrossRef](#)]
28. Wu, H.; Jiang, L.; Zhong, X.; Liu, J.; Qin, N.; Qian, L. Exploring the role of $-NH_2$ functional groups of ethylenediamine in chemical mechanical polishing of GCr15 bearing steel. *Friction* **2021**, *9*, 1673–1687. [[CrossRef](#)]
29. Zhou, G.; Guo, J.; Zhao, J.; Tang, Q.; Hu, Z. Nanoindentation Properties of 18CrNiMo7-6 Steel after Carburizing and Quenching Determined by Continuous Stiffness Measurement Method. *Metals* **2020**, *10*, 125. [[CrossRef](#)]
30. Wu, J.; Wei, P.; Liu, H.; Zhang, B.; Tao, G. Effect of shot peening intensity on surface integrity of 18CrNiMo7-6 steel. *Surf. Coat. Technol.* **2021**, *421*, 127194. [[CrossRef](#)]
31. Sun, D.; Guo, Z.; Gu, J. The microstructure and crystallography of lath martensite with Greninger-Troiano orientation relationship in a Fe-12.8Ni-1.5Si-0.22%C steel. *Mater. Charact.* **2021**, *181*, 111501. [[CrossRef](#)]
32. Moschona, A.; Plesu, N.; Mezei, G.; Thomas, A.G.; Demadis, K.D. Corrosion protection of carbon steel by tetraphosphonates of systematically different molecular size. *Corros. Sci.* **2018**, *145*, 135–150. [[CrossRef](#)]
33. Delahay, P.; Pourbaix, M.; Van Rysselberghe, P. Potential-pH diagrams. *J. Chem. Educ.* **1950**, *27*, 683. [[CrossRef](#)]
34. Kubal, M.; Panacek, F. Potential-pH diagram for Fe-H₂O-citric acid system. *Br. Corros. J.* **1995**, *30*, 309–311. [[CrossRef](#)]
35. Beverskog, B.; Puigdomenech, I. Revised pourbaix diagrams for iron at 25–300 °C. *Corros. Sci.* **1996**, *38*, 2121–2135. [[CrossRef](#)]
36. Small, L.; Brumbach, M.; Apblett, C.; Ihlefeld, J.F.; Brennecke, G.; Duquette, D. On the Degradation Processes of Thin Film PZT in 0.1 N H₂SO₄. *J. Electrochem. Soc.* **2013**, *160*, C128–C135. [[CrossRef](#)]
37. Liu, T.; Li, T.; Liu, X. TEM and electron diffraction analysis of ω -Fe to cementite transformation in quenched and tempered high carbon steels. *AIP Adv.* **2019**, *9*, 045219. [[CrossRef](#)]
38. Fan, Q. A new method of calculating interplanar spacing: The position-factor method. *J. Appl. Crystallogr.* **2012**, *45*, 1303–1308. [[CrossRef](#)]
39. Cheng, L.; Böttger, A.; de Keijser, T.H.; Mittemeijer, E.J. Lattice parameters of iron-carbon and iron-nitrogen martensites and austenites. *Scr. Metall. Mater.* **1990**, *24*, 509–514. [[CrossRef](#)]
40. Biesinger, M.C.; Payne, B.P.; Grosvenor, A.P.; Lau, L.W.M.; Gerson, A.R.; Smart, R.S.C. Resolving surface chemical states in XPS analysis of first row transition metals, oxides and hydroxides: Cr, Mn, Fe, Co and Ni. *Appl. Surf. Sci.* **2011**, *257*, 2717–2730. [[CrossRef](#)]
41. Mills, P.; Sullivan, J.L. A study of the core level electrons in iron and its three oxides by means of X-ray photoelectron spectroscopy. *J. Phys. D Appl. Phys.* **1983**, *16*, 723–732. [[CrossRef](#)]
42. Grosvenor, A.P.; Kobe, B.A.; Biesinger, M.C.; McIntyre, N.S. Investigation of multiplet splitting of Fe 2p XPS spectra and bonding in iron compounds. *Surf. Interface Anal.* **2004**, *36*, 1564–1574. [[CrossRef](#)]
43. Keller, P.; Strehlow, H.-H. XPS investigations of electrochemically formed passive layers on Fe/Cr-alloys in 0.5 M H₂SO₄. *Corros. Sci.* **2004**, *46*, 1939–1952. [[CrossRef](#)]
44. Barroux, A.; Duguet, T.; Ducommun, N.; Nivet, E.; Delgado, J.; Laffont, L.; Blanc, C. Combined XPS / TEM study of the chemical composition and structure of the passive film formed on additive manufactured 17-4PH stainless steel. *Surf. Interfaces* **2021**, *22*, 100874. [[CrossRef](#)]

45. El-Katori, E.E.; Nessim, M.I.; Deyab, M.A.; Shalabi, K. Electrochemical, XPS and theoretical examination on the corrosion inhibition efficacy of stainless steel via novel imidazolium ionic liquids in acidic solution. *J. Mol. Liq.* **2021**, *337*, 116467. [[CrossRef](#)]
46. Xu, L.; Wang, J. A heterogeneous Fenton-like system with nanoparticulate zero-valent iron for removal of 4-chloro-3-methyl phenol. *J. Hazard. Mater.* **2011**, *186*, 256–264. [[CrossRef](#)]
47. Du, C.W.; Li, X.G.; Liang, P.; Liu, Z.Y.; Jia, G.F.; Cheng, Y.F. Effects of Microstructure on Corrosion of X70 Pipe Steel in an Alkaline Soil. *J. Mater. Eng. Perform.* **2009**, *18*, 216–220. [[CrossRef](#)]
48. De Laat, J.; Le, T.G. Effects of chloride ions on the iron(III)-catalyzed decomposition of hydrogen peroxide and on the efficiency of the Fenton-like oxidation process. *Appl. Catal. B Environ.* **2006**, *66*, 137–146. [[CrossRef](#)]
49. Kim, Y.J.; Kwon, O.J.; Kang, M.C.; Kim, J.J. Effects of the Functional Groups of Complexing Agents and Cu Oxide Formation on Cu Dissolution Behaviors in Cu CMP Process. *J. Electrochem. Soc.* **2011**, *158*, H190. [[CrossRef](#)]
50. Chu, C.M.; Wan, C.C. Effect of citric acid as a chelating agent on anodic behavior of pure iron with potentiostatic polarization and cyclic voltammetry methods. *Mater. Chem. Phys.* **1993**, *33*, 189–196. [[CrossRef](#)]
51. Choi, S.; Tripathi, S.; Dornfeld, D.A.; Doyle, F.M. Copper CMP Modeling: Millisecond Scale Adsorption Kinetics of BTA in Glycine-Containing Solutions at pH 4. *J. Electrochem. Soc.* **2010**, *157*, H1153. [[CrossRef](#)]
52. Tripathi, S.; Choi, S.; Doyle, F.M.; Dornfeld, D.A. Integrated Tribo-Chemical Modeling of Copper CMP. *MRS Online Proc. Libr.* **2010**, *1157*, 203. [[CrossRef](#)]
53. Liu, L.; Zhang, Z.; Wu, B.; Hu, W.; Meng, F.; Li, Y. A review: Green chemical mechanical polishing for metals and brittle wafers. *J. Phys. D Appl. Phys.* **2021**, *54*, 373001. [[CrossRef](#)]
54. Liu, J.; Jiang, L.; Xiao, G.; Qian, L. High-performance chemical mechanical polishing of GCr15 bearing steel enabled by the synergistic action of oxalic acid and H₂O₂. *J. Solid State Electrochem.* **2022**, *26*, 809–820. [[CrossRef](#)]
55. Liu, J.; Jiang, L.; Wu, H.; Zhao, T.; Qian, L. 5-Methyl-1H-Benzotriazole as an Effective Corrosion Inhibitor for Ultra-Precision Chemical Mechanical Polishing of Bearing Steel. *J. Electrochem. Soc.* **2020**, *167*, 131502. [[CrossRef](#)]
56. Liu, J.; Jiang, L.; Qian, L. Achievement of sub-nanometer surface roughness of bearing steel via chemical mechanical polishing with the synergistic effect of heterocyclic compounds containing N and S. *J. Appl. Electrochem.* **2022**, *52*, 357–373. [[CrossRef](#)]
57. Peng, Y.; Shen, B.; Wang, Z.; Yang, P.; Yang, W.; Bi, G. Review on polishing technology of small-scale aspheric optics. *Int. J. Adv. Manuf. Technol.* **2021**, *115*, 965–987. [[CrossRef](#)]